

Numerical study on drop formation in single hole in solvent extraction

A. Soleymani, A. Laari, I. Turunen

Department of Chemical Technology, Lappeenranta University of Technology, Laboratory of Process and Product Development, PO Box 20, 53851 Lappeenranta, Finland

Abstract

In the present study, computational fluid dynamics (CFD) simulation were performed to investigate the drop formation in single holes in a solvent extraction. The effects of various operating and design parameters on the drop formation were investigated in order to optimize the drop formation. Simulation results indicated that CFD simulations can give useful information about the drop formation in sieve plates. According to the numerical results, clearly different drop formation periods were detected. These periods were essentially different for the straight and conical holes. Furthermore, it was shown that the shape of the hole have considerable effect to the size of the drops formed. The simulation results were verified by comparison to experimental observations obtained using high-speed video technology. The numerical results of the drop shapes and detachment times were found to be consistent with images of experimental drops across a wide range of solute volume flow rates.

Keywords: computational fluid dynamics, drop formation, single hole, contact angle, VOF.

1. Introduction

Formation of solvent drops in sieve plates is a very important phenomenon in solvent extraction. Small droplets are usually desired to increase the interfacial area available for mass transfer and to maximize the process efficiency. Formation of very small satellite drops is, however, a common problem, which is frequently met in industrial extraction equipment. Very small droplets are difficult to separate from the continuous phase and their presence can adversely affect extraction efficiency. Formation of satellite drops can be affected by changes in flow conditions and in the mechanical structure of the sieve plates. Drop formation in sieve plates is a complex phenomenon, which depends on the flow velocity in the holes, physical properties of the liquid phases, like surface tension and density difference, material properties of

the sieve plate such as the wetting properties and surface roughness, size and structure of the hole, distance between the holes and alignment of holes on the sieve plate.

Over the past decade, computational methods have proven to be an effective tool to study the process in which the multiphase flow takes place. Simulation of multiphase flow along surfaces is a frequently met phenomenon in industrial processes, for example in catalysis, phase dispersion, boiling and cavitation etc. Different methods for the tracking of interface in free surface flows have been developed. They include the Marker-and-Cell, Front-Tracking, Lattice-Boltzmann, Level Set and Volume of Fluid (VOF) methods. In most of the abovementioned methods there are severe disadvantages, such as large requirement for computer memory or long calculation times, which make the practical use of these methods difficult. In contrast, the VOF method presented by Hirt and Nichols (1981) is considered to be computationally efficient. This method has been recently successfully used for the calculation of different multiphase flow cases.

Hoffmann et al. (2006) and Gu et al. (2000) have simulated liquid rivulet flow along inclined plate. Gunjal et al. (2003) have simulated the impact of drop on solid surface. Ataki and Bart (2004, 2006) used the VOF method to calculate wetting of a structured packing element and flow of liquid rivulet along flat and wavy inclined plates. Biń et al. (2006) have studied the formation of bubble in a stagnant or cross-flowing liquid using the VOF method. Ohta et. al (2004) have used a coupled level-set/volume-of fluid (CLSVOF) method for the calculation of the movement of rising bubbles.

The models and results for the formation and flowing of dispersed phase particles in fluids are mostly presented for gas-liquid phases. Among the limited number of studies presented for liquid drop formation in a liquid continuous phase are the work of Ohta et al. (1995) and Richards et al. (1995). Ohta et al. (1995) have simulated drop formation in a hole in a pulsed sieve plate using the VOF method. In their case, the calculational domain was two-dimensional and axisymmetry was assumed. Richards et al. (1995) have simulated drop formation in liquid-liquid systems before and after jetting conditions.

In the present study, computational fluid dynamics type simulation was performed to study the drop formation process resulted from the feeding of a liquid phase through a single hole as schematically shown in Fig. 1. The continuous and dispersed phases are assumed to be immiscible liquids. The objective of this study was to search for optimal conditions for drop formation in single hole by minimizing the production of very small satellite drops aiming simultaneously to small drop sizes and high mass transfer efficiency. The effects of various operating and design parameters, such as volume flow rate, the hole size, the structure of the hole or the construction material of the sieve plate on the drop formation were studied.

2. Configuration of the apparatus

The schematic picture of the test devices used in the present study is shown in Fig. 1. The column of diameter $D = 23$ mm and height $h = 38$ mm was initially filled with continuous phase, and the dispersed phase was fed to the column through a single hole.

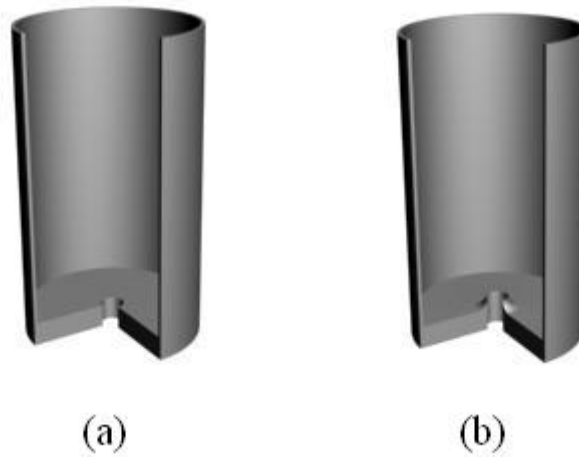


Fig.1 The schematic picture of the test device used in this study. A 90° slice has been removed for the better visualizations. (a) straight hole, (b) hole with a conical opening facing upwards.

As illustrated in Fig. 2, two different configurations for the hole were used to investigate the influence of the structure of the hole in the drop formation. Moreover, the hole diameter was varied. The detail dimensions of the holes are depicted in Fig. 2.

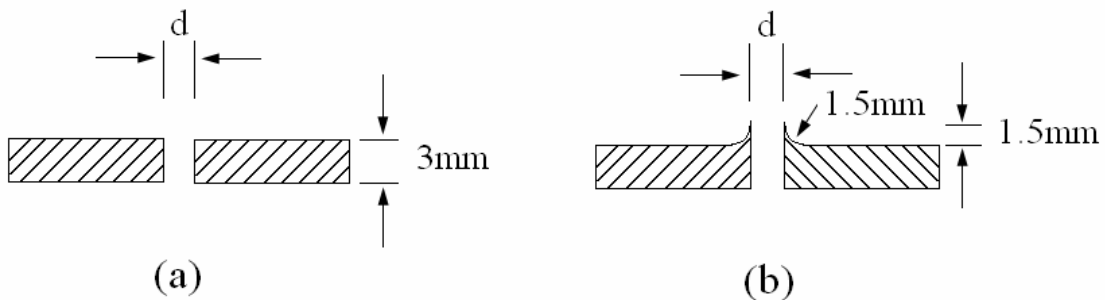


Fig. 2. The schematic diagram of the structure of the hole of the test column. (a) straight hole, (b) hole with a conical opening facing upwards.

3. Experiments

In order to verify the numerical calculations, a series of experiments were performed to visualize the drop formation process. The droplets were formed at the outlet of the hole with diameter of 3 mm. The construction material for the plate and the hole was stainless steel. The column was initially filled with de-ionized water and at instant $t = 0$, the Exxol D80 (dispersed phase) was injected to the column from the hole. The superficial velocity of the disperse phase was varied within the range of 3-21 cm/sec. The images of the forming droplets were recorded by a high-speed digital video camera with time resolution of 200 frames per second.

3.1. Measuring the contact angle

The contact angle was obtained photometrically by measuring at rest the angle between the drop in the hole and the plate. The value obtained for Exxol D80-water and steel plate was 67° . This value was used in the simulations.

4. Simulation method

Computational Fluid Dynamics type simulation was carried out with the commercial code FLUENT 6.3.26 (ANSYS Inc.). The volume of fluid (VOF) model was applied to capture the drop formation of a solute liquid injected from a single hole to a column initially filled with a liquid solvent. The surface tension along the interface between two phases was implemented using the continuum surface force (CSF) model proposed by Brackbill et al [1992]. The continuous and dispersed phases are assumed to be immiscible liquids. The physical properties of the phases used in both simulations and experiments are presented in Table1.

Table1. Physical properties of the fluids used in both simulations and experimentations at 25 °C

phase	density kg/m ³	liquid-air surface tension mN/m	viscosity mPa s
continuous phase (water)	998	72.0	0.89
dispersed phase (Exxol D80)	796	26.3	1.74

4. 1. Governing equations

According to the VOF model a single momentum equation is solved throughout the domain, and the resulting velocity field is shared among the phases. The mass and momentum conservation equations for the two-phase flow throughout the domain are then described by

$$\frac{\partial}{\partial t} \rho + \nabla \cdot \rho \mathbf{V} = 0, \quad (1)$$

$$\frac{D}{Dt} \rho \mathbf{V} = -\nabla P + \nabla \cdot \left[\mu \left(\nabla \mathbf{V} + (\nabla \mathbf{V})^T \right) \right] + \rho \mathbf{g} + \mathbf{F}_{ST}. \quad (2)$$

where \mathbf{V} is the velocity vector, t is the time, P is the pressure, and \mathbf{g} is the gravitational acceleration. The conservative equations (1) and (2) are dependent on the volume fractions of both phases through the properties ρ and μ , defined as

$$\rho = \sum \rho_q \phi_q \quad (3)$$

$$\mu = \sum \mu_q \phi_q \quad (4)$$

Subscript q represents the phases and ϕ is the volume fraction. The term \mathbf{F}_{ST} is the surface tension force per unit volume, which can be introduced in the momentum equation following the continuum surface force (CSF) model of Brackbill et al [1992] as

$$\mathbf{F}_{ST} = \sigma \kappa \mathbf{n} \delta \quad (5)$$

Here κ is the mean curvature, \mathbf{n} is the unit normal vector of the interface and δ is the interface delta function. σ is the surface tension coefficient between the liquids pair which can be calculated as

$$\sigma_{\alpha,\beta} = \sigma_\alpha + \sigma_\beta - \sqrt{\sigma_\alpha \sigma_\beta} \quad (6)$$

where σ_α and σ_β are the surface tension coefficients between phases α -air and β -air, respectively. Using Eq (6) a value of 54.8×10^{-3} N/m is obtained for the surface tension between the continuous and the dispersed phases.

The surface curvature κ was computed from the local gradients in the surface normal at the interface. The contact angle, defined as the angle between the wall and the tangent to the interface at the wall, was implemented to adjust the curvature of the interface near the wall.

4. 2. Boundary and initial conditions

To reduce the computational time a two-dimensional coordinate system was used. A uniform velocity profile ranging from 3-14 cm/sec was assumed at the inlet of the hole and the pressure at the exit of the column was assumed to be fixed to the local atmospheric pressure. No-slip boundary condition at the side walls was applied and the boundary condition on the volume fraction of the dispersed phase at the inlet of the hole was set to 1. In this set of simulations the column was initially filled with the continuous phase (water). The dispersed phase (Exxol D80) was then introduced from the hole. The time dependent computations were carried out until the pseudo-steady state conditions were reached.

4. 3. Simulation Scheme

The whole domain was discretized using 100,000 quadrilateral elements to predict the drop formation of the dispersed phase correctly. Finer grids were used in the vicinity of the axis of the column. The fields of the velocity and volume fraction in the column as schematically illustrated in Fig. 1 were sought through discretization using finite volume formulation (Patankar, 1980). The integral forms of the governing equations 1 and 2 were considered at each element of a large number of quadrilateral elements to produce a set of coupled nonlinear algebraic equations using the second order upwind differencing scheme for momentum discretization in conjunction with a first-order implicit-in-time discrete differentiation. These equations are linearized and solved using the PISO (Pressure-Implicit with Splitting of Operators) algorithm.

5. Results and discussion

Simulations were performed to investigate the effects of volume flow rate, hole size and hole structure on the drop formation in the column shown in Fig. 1. The superficial velocity in the hole was varied from 3 to 14 cm/s.

5. 1. Validation of numerical results

The numerical results were compared with the data obtained from the experiments to validate the simulation method. Fig. 3 and Fig. 4 illustrate the temporal evolution of the drop shapes for the lowest and highest values of the superficial velocities of the dispersed phase used in the simulation. As shown from Fig. 3 and Fig. 4, there is a good agreement between the results obtained from numerical calculations and experimental results for the drop shapes.

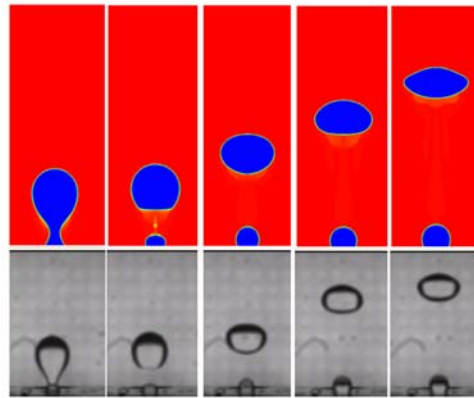


Fig. 3. Temporal evolution of the drop shapes resulted from numerical calculations (Top row), and experimental study (bottom row). The diameter of the hole was 3 mm and the superficial velocity of the liquid fed to the hole was 3 cm/s.

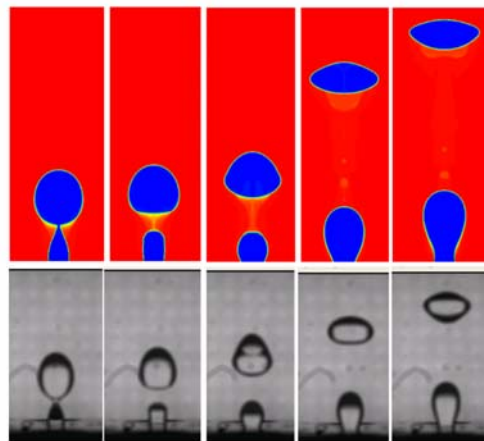


Fig. 4. Temporal evolution of the drop shapes resulted from numerical calculations (Top row), and experimental study (bottom row). The diameter of the hole was 3 mm and the superficial velocity of the liquid in the hole was 14 cm/s.

5. 2. Drop formation dynamics

Fig. 5 shows the sequence of the drop formation in the vicinity of the straight hole for the superficial velocity of 14 cm/sec. The simulation results show that the mechanisms of the drop formation for the straight holes are similar regardless to hole size or volume flow rates in the range of the velocities studied. As illustrated in Fig. 5, four main periods can be distinguished over the formation of a drop namely, separation, spreading, growth and necking periods.

The period of *separation* starts just after detachment of a drop. During this stage the height of the drop decreases and it starts spreading. During the stage of *spreading*, the

base of drop starts spreading along the plate. At the end of this period, the base of the drop reaches to its maximum value. Meanwhile, there is a slight decrease of drop height. Just after the end of the spreading period, in the beginning of the *growth* period the drop base starts decreasing. Though the height of the drop increases during this period, its maximum width doesn't change considerably. At the stage of *necking*, the drop becomes elongated and expands continuously while moving upwards. During this last stage, the neck formation begins and at the end of this stage the drop detaches.

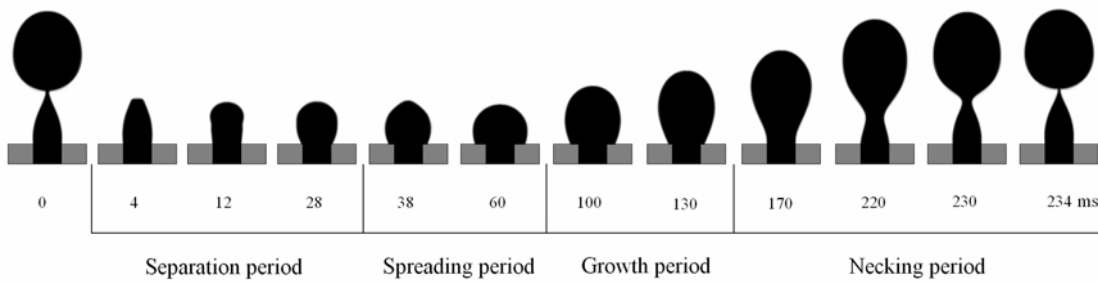


Fig. 5. Four main periods of the drop evolution for $d=3$ mm and $u=14$ cm/s

Fig. 6 illustrates the schematic picture of a drop in the vicinity of the hole. Using the symbols shown in Fig. 6, the mathematical description of the four main stages of the drop formation is summarized in table 2.

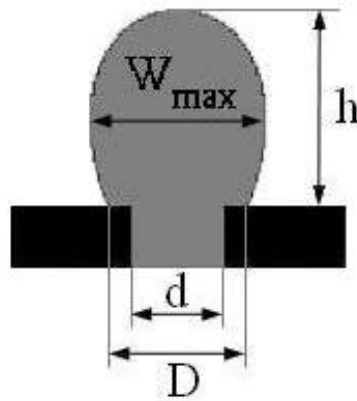


Fig. 6. Drop image in the vicinity of the hole and its dimensions

Table 2. Mathematical definition of the main periods of the drops formation in the hole

Separation period	$\partial D/\partial t = 0$ ($D = d$)	$\partial W_{\max}/\partial t > 0$	$\partial h/\partial t < 0$
Spreading period	$\partial D/\partial t > 0$	$\partial W_{\max}/\partial t > 0$	$\partial h/\partial t < 0$
Growth period	$\partial D/\partial t < 0$	$\partial W_{\max}/\partial t \cong 0$	$\partial h/\partial t > 0$
Necking period	$\partial D/\partial t = 0$ ($D = d$)	$\partial W_{\max}/\partial t > 0$	$\partial h/\partial t > 0$

Fig. 7 presents the stages of the drop formation in the vicinity of the conical hole with a diameter of 3 mm. As depicted in Figs. 5 and 7, the differences between the stages of drop formation in a straight and conical hole are revealed. Based on the definition of each period summarized in table 2, the spreading and growth periods do not exist and the time of the necking period significantly increases.

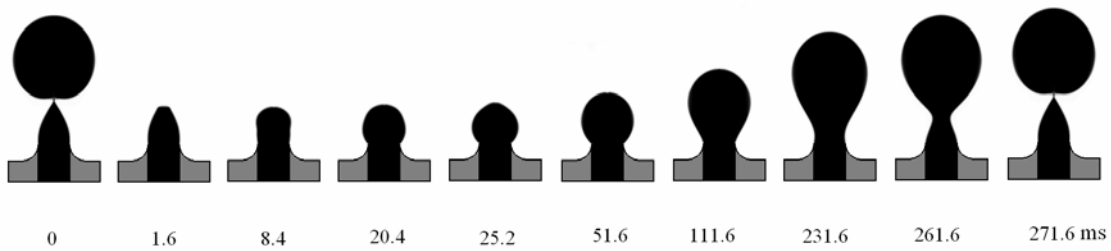


Fig. 7. The sequence of the drop formation in the vicinity of a hole with a conical opening facing upwards for $d=3$ mm and $u=14$ cm/sec.

5. 3. Time interval between the detachment of two successive drops

Fig. 8 shows the numerical results of time interval between the detachments of two successive drops as a function of inlet superficial velocity. The effects of the hole size and the structure of the hole on the drop formation were studied by considering two straight holes of diameters of 2 and 3 mm and a conical hole of diameter 3 mm.

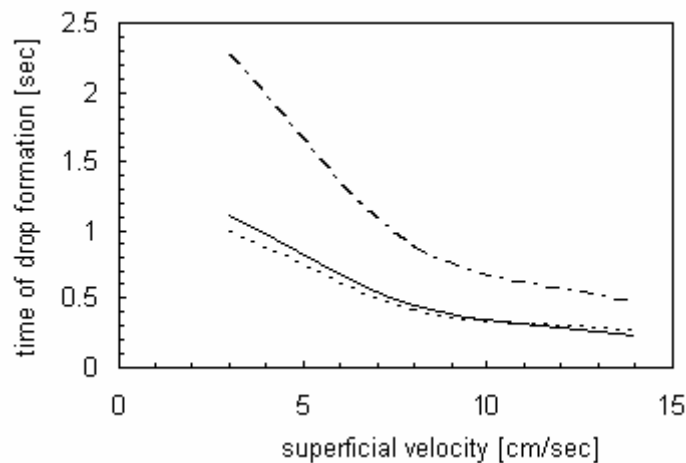


Fig. 8. Effect of inlet superficial velocity of on the time interval between the detachment points of two successive drops. The solid, dashed-dotted and dotted lines represent the profile of drop formation time for straight hole of diameter 3 mm, straight hole of diameter 2 mm and conical hole of diameter 3 mm, respectively.

As depicted in Fig. 8 in the studied range of velocities the trends are the same for all the holes. As the velocity increases, the time interval between the detachments of two successive drops decreases. Increase of the hole size results in the deduction of the required time for the formation of a drop. From Fig. 8, it can be concluded that the hole structures studied here do not have a significant effect on the time of drop formation.

5. 4. Separation distance

Fig. 9 presents the variation of the distance of the detachment point of a drop from the hole with superficial velocity. Again the same trends were observed for the holes. The separation distance varies linearly with the velocity. Increase of the superficial velocity results in an increase of the separation distance of a drop. As shown in Fig. 9, a decrease of the hole diameter from 3 mm to 2 mm results in 50% decrease of the separation distance. Furthermore, the simulation results reveal that in the column with the conical hole the separation distance is larger than for in the straight hole with the same diameter.

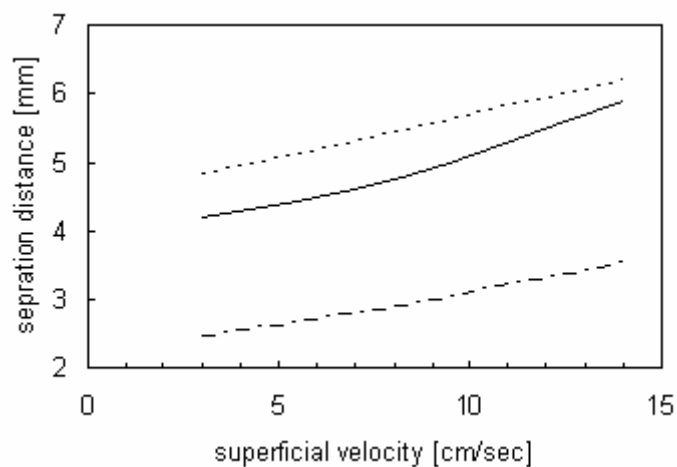


Fig. 9. Distance of the detachment point of a drop from the hole as a function of inlet superficial velocity. The solid, dashed-dotted and dotted lines represent the profile of drop formation time for straight hole of diameter 3mm, straight hole of diameter 2mm and conical hole of diameter 3mm, respectively.

5. 5. Shape and size of the detached drop

Fig. 10 presents the curves relating the drop aspect ratio in the detachment point to the inlet superficial velocity. Here the aspect ratio is defined as the ratio of the drop height to its maximum width and it describes the sphericity of the drop. The results

indicate that the increase of the superficial velocity leads to more deviation from spherical shape. Increase of the hole size results in a decrease of the aspect ratio. From Fig. 10, it can be concluded that the conical hole produces more spherical drops than the straight hole with the same diameter.

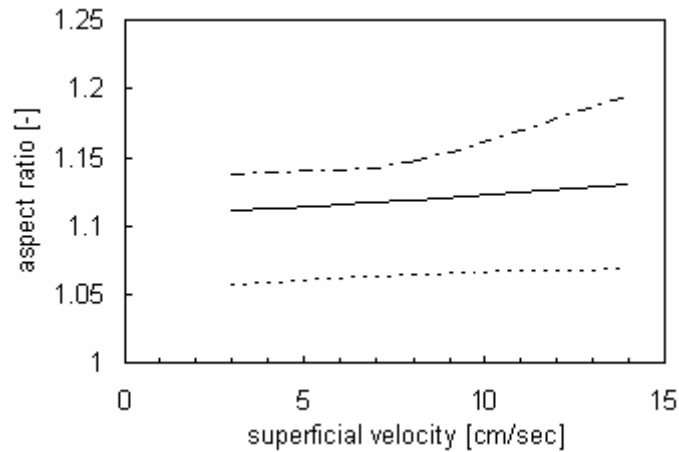


Fig. 10. Variation of the aspect ratio of the detached drop with superficial velocity. The solid, dashed-dotted and dotted lines represent the profile of drop formation time for straight hole of diameter 3mm, straight hole of diameter 2mm and conical hole of diameter 3mm, respectively.

The equivalent diameter of the detached drop is shown as a function of superficial velocity in Fig. 11. The results indicate that the trends are different for the straight holes and conical holes. The equivalent diameter increases with velocity. Increase of the straight hole diameter leads to the larger equivalent diameter of the drop. Furthermore from the simulation results it can be concluded that for a constant velocity and hole diameter, the conical hole produces drops with smaller equivalent diameters.

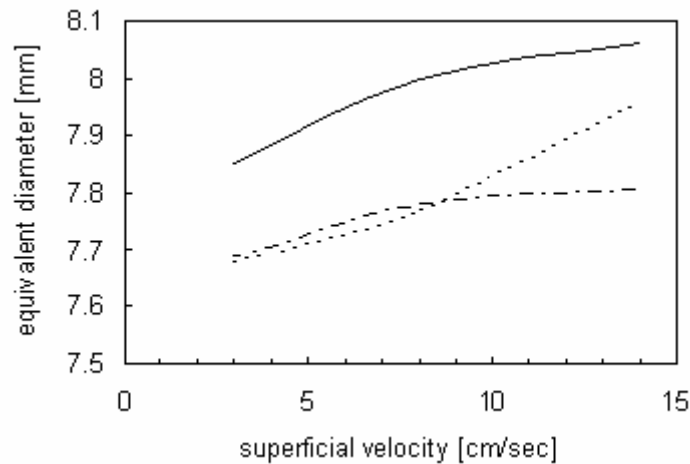


Fig. 11. Equivalent diameter of the detached drop versus superficial velocity. The solid, dashed-dotted and dotted lines represent the profile of drop formation time for straight hole of diameter 3mm, straight hole of diameter 2mm and conical hole of diameter 3mm, respectively.

Conclusions

According to the simulation results, clearly different drop formation periods were detected. These periods were essentially different for the straight and conical holes.

Simulation results revealed that the straight holes produce drops with larger equivalent diameter compared to the conical holes of the same size. Moreover, the time interval between the detachments of two successive drops is roughly the same for both the straight and the conical holes with the same hole diameter and volume flow rate.

It was shown that the equivalent drops diameters produced with the straight hole of diameter 3 mm are larger than those produced with the straight hole of diameter 2 mm. Also it was shown that the time of drop formation decreases with an increase in the diameter of the straight hole.

Regardless of the hole structure or size, the simulation results showed that an increase of the superficial velocity results in a decrease of drop formation time and an increase in the equivalent diameter of the drop. It should be noted that all the achieved results are valid for the ranges of volume flow rate and structural parameters used in this study.

The surface tension and contact angle play important roles in the drop formation. In regard to this it merits to investigate the effect of the various liquid-liquid pairs and construction materials of the hole. Moreover, in the course of drop growth and rising, it is important to investigate the temporal evolution of the drop interfacial area and its residence time in the column, since these parameters largely determine the rate of mass transfer. These issues will be the subject of a future paper.

References

Ataki, A., Bart, H.-J., Experimental and CFD Simulation Study for the Wetting of a Structured Packing Element with Liquids, *Chem. Eng. Technol.*, Vol. 29 (2006), 336-347.

Ataki, A., Bart, H.-J., The Use of VOF-Model to Study the Wetting of Solid Surfaces, *Chem. Eng. Technol.*, Vol. 27 (2004), 1109-1114.

Bico, J., Thiele, U., Quéré, D., Wetting of textured surfaces, *Colloids and Surfaces A: Physicochemical and Engineering Aspects*, 206 (2002), 41-46.

Biń, A., Machniewski, P., Rudniak, L., Numerical simulation of bubble formation in stagnant and cross-flowing liquids, *Inżynieria Chemiczna i Procesowa*, Vol. 27 (2006), 287-303.

Brackbill, J. U., Kothe, D. B., Zemach, C., A continuum method for modelling surface tension, *Journal of Computational Physics*, Vol. 100 (1992), 335-354.

Böhringer, K. F., "Towards Optimal Strategies for Moving Droplets in Digital Microfluidic Systems." *IEEE International Conference on Robotics and Automation (ICRA)*, New Orleans, April 26 - May 1, 2004.

Gnyloskurenko, S., V., Byakova, A. V., Raychenko, O. I., Nakamura, T., Influence of wetting conditions on bubble formation at orifice in a inviscid liquid: Transformation of bubble shape and size, *Colloids and Surfaces A: Physicochem. Eng. Aspects*, 218 (2003), 73-87.

Gu, F., Liu, C. J., Yuan, X. G., Yu, G. C., CFD simulation of liquid film flow on inclined plates, *Chem. Eng. Technol.*, 27 (2004), 1099-1104.

Gunjal, P. R., Ranade, V. V., Chaudhari, R. V., Experimental and computational study of liquid drop over flat and spherical surfaces, *Catalysis Today*, 79-80 (2003), 267-273.

Gunjal, P. R., Ranade, V. V., Chaudhari, R. V., Dynamics of drop impact on solid surface: Experiments and VOF simulations, *A. I. Ch. E. J.*, 51 (2005), 59-78.

Hirt, C. W., Nichols, B. D., Volume of fluid method for the dynamics of free boundaries, *J. Comput. Phys.*, Vol 39 (1981), 201-225.

Hoffmann, A., Ausner, I., Repke, J.-U., Wozny, G., Detailed investigation of multiphase (gas-liquid and gas-liquid-liquid) flow behaviour on inclined plates, *Chem. Eng. Res. Des.*, 84(A2) (2006), 147-154.

Hoffmann, A., Ausner, I., Repke, J.-U., Wozny, G., Fluid dynamics in multiphase distillation processes in packed towers, *Computers and Chemical Engineering*, Vol. 29 (2005), 1433-1437.

Martín, M., Montes, F. J., Galán, M. A., Numerical calculation of shapes and detachment times of bubbles generated from a sieve plate, *Chem. Eng. Sci.*, 61 (2006), 363-369.

Ohta, M., Yamamoto, M., Suzuki, M., Numerical analysis of a single drop formation process under pressure pulse condition, *Chem. Eng. Sci.*, 50 (1995), 2923-2931.

Ohta, M., Haranaka, S., Yoshida, Y., Sussman, M., Three-dimensional numerical simulation of the motion of a gas bubble rising in viscous liquids, *J. Chem. Eng. Japan*, Vol. 37 (2004), 968-975.

Patankar S. V., *Numerical heat transfer and fluid flow*, McGraw-Hill, New York (1980).

Richards, J. R., Beris, A. N., Lenhoff, A. N., Drop formation in liquid-liquid systems before and after jetting, *Phys. Fluids.*, Vol. 11 (1995), 2617-2630.

Shastri, A., Case, M. J., Böhringer, K. F., Engineering Surface Roughness to Manipulate Droplets in Microfluidic Systems, *IEEE Conference on Micro Electro Mechanical Systems (MEMS)*, Miami Beach, FL, January 30 – February 3, 2005.